CYCLIC LOADING TESTS OF SLENDER CONCRETE MASONRY SHEAR WALLS

M.J.N. Priestley*, D.McG. Elder**

SUMMARY:

The design, construction and testing of three slender concrete masonry shear walls is reported. The three walls, modelling 190 mm thick blockwork walls of four to five stories height to a scale of 1:0.737 were subjected to cyclic reversals of in-plane displacements at gradually increasing ductility factors, simulating the effects of seismic loading. Variables between walls included axial load level, and whether or not confining plates were placed in the mortar beds in the compression zones of the potential plastic hinge region. All walls were constructed by conventional methods, and included lapped starter bars within the plastic hinge.

Results indicated that the unconfined walls suffered strength degradation at levels of ductility lower than those required by current ductile design practice. This was particularly the case for the wall with heavy axial loading, and confirmed theoretical predictions of available ductility based on a limiting ultimate compression strain of 0.25%. Response of the confined wall exhibited greatly improved behaviour compared with an otherwise identical unconfined wall. In all walls behaviour was significantly, and adversely, affected by the lapping of flexural steel at the wall base.

INTRODUCTION:

Over recent years there has been considerable research activity into the seismic performance of masonry shear walls. However, the work relevant to New Zealand design needs has been on squat cantilever walls (aspect ratio $h_w/\ell_w < 2$)[1-4] or on masonry piers[5,6]. Little attention has been paid to masonry shear walls of high aspect ratio, on the assumption that conditions for such walls will be more conducive to ductile behaviour than for squat walls. Research on squat walls has indicated that ductile flexural failure modes can be obtained, with brittle shear failures inhibited, by use of a capacity design approach[1-2]. Adequate ductility was obtained, but considerable stiffness, and to a lesser extent strength, degradation resulted from the shear walls sliding on the foundation beam unless axial load levels were high. Since slender walls are less likely to be affected by base-sliding than squat walls, the satisfactory performance from squat walls has been widely taken to indicate that adequate ductility will also be available from more slender walls.

Examination of the theoretical behaviour of slender masonry walls reveals that this assumption is not necessarily valid. Three factors conspire to make conditions for slender walls more critical than corresponding squat walls, as discussed in the subsequent sections.

Ductility Limits Imposed by Unconfined Masonry -

In a recent paper[7], aspects of the theoretical ductility capacity of unconfined masonry shear walls were discussed. Based on the assumption that the plastic hinge length L_p at the wall base had the value $L_p = 0.5L_w$ regardless of wall height, it was shown that the available ductility μ was given by the expression

$$\mu = 1 + \frac{1.5}{A_e}\left(\frac{\phi_u}{\phi_y} - 1\right)\left(1 - \frac{1}{4A_e}\right) \qquad (1)$$

Where $A_e = h_e/\ell_w$ was the effective wall aspect ratio, ϕ_u was the ultimate curvature, and ϕ_y was the yield curvature, assuming elasto-plastic response.

Since ϕ_u and ϕ_y will be constant for a given wall section, reinforcement layout and axial load level, it follows from Eq. (1) that the available displacement ductility μ will decrease with increasing aspect ratio. Design charts were presented in reference 7 to enable actual ductility capacity of rectangular shear walls to be estimated. These indicated that in many real situations, available ductility would be less than the commonly accepted value of $\mu = 4$ for slender ductile shear walls.

Instability of Compression Zone

There is a potential for lateral instability of the compression zone of masonry walls, particularly within plastic hinge regions. Although to our knowledge no experimental data are available to establish critical values of parameters affecting potential for instability for walls, it is apparent that the ratio of unsupported height to wall width must be significant, and that in walls where the neutral axis depth in the plastic hinge zone is a small fraction of the wall length, the compression zone is unlikely to buckle, because of support provided by the greater part of the wall, that is in tension.

In the absence of experimental data pertaining to walls, the draft New Zealand concrete design code[8] has adopted rules

* Reader in Civil Engineering, University of Canterbury
**Graduate Student, Oxford University

for stability of columns, modified by the above arguments. The requirements may be summarised as follows:

(i) Walls less than three storeys in height need not be subject to special instability rules within plastic hinge regions. This recognises the fact that in one or two storied walls the vertical spread of plasticity will be only a fraction of the unsupported storey height, and instability will be unlikely.

(ii) For walls of three storeys or higher, the thickness, b_w, of wall located in the region from the extreme compression fibre to the section midway to the neutral axis, must not be less than $\ell_n/10$, where ℓ_n is the unsupported storey height, unless

(a) the computed neutral axis depth c is less than $4\ b_w$ or $0.3\ \ell_w$

or

(b) the compression zone is stabilized by a flange or cross wall within a distance of $3\ b_w$ from all parts of the region governed by the width requirement.

The draft New Zealand masonry design code[9] has incorporated similar requirements, except that the wall width required under item (ii) above is $0.075\ \ell_n$ rather than $0.1\ \ell_n$. Compliance with these requirements can create difficulties. Even with an unsupported storey height of 2.8 m, which is about the minimum feasible, a wall width of 210 mm would be required unless the neutral axis depth was small. Thus 190 mm blockwork could not be used.

Since most masonry structures will be designed for 8 MPa (the default option for Grade A masonry unless prism tests are carried out, and the standard value for Grade B masonry[9]) the requirements of $c < 4\ b_w$ and $c < 0.3\ \ell_w$ will be hard to meet, and use of uneconomical 240 mm blockwork would frequently be necessary to satisfy code requirements for masonry walls of three or more storeys.

Lapping of Reinforcement in Potential Plastic Hinge Zones -

Lapping of flexural reinforcement with vertical starter bars in potential plastic hinge zones is clearly undesirable as conditions for bond, under cyclic reversals of yield stress, are extremely severe. Such lapping is not permitted in the draft concrete design code[8] but is allowed in the draft masonry design code[9], because of construction difficulties in threading blocks onto starter bars extending up beyond the potential plastic hinge region (typically one storey height). The draft masonry code[9] recommends that wherever possible the undesirable practice of lapping in hinge zones be avoided by spacing vertical reinforcement at 400 mm centres and using open-end blocks layed with the open end alternately to left and right on alternate courses. That is, the reinforcement is always in an open core. With such a design the blocks can be moved horizontally into position rather than threaded onto the starters, and no particular difficulties need then be experienced with tall starters. This method, however is not suitable where high reinforcement ratios indicate a requirement for bars at 200 centres.

Although squat walls previously tested[1-3] have included lapped vertical bars, the moment gradient over the lap has been substantial, so bond conditions have not been severe. With tall walls the entire lap will be subject to almost constant moment, and bond breakdown is much more likely to occur.

The research reported in this paper was set up to investigate the influence of the above factors on the response of slender concrete masonry walls to simulated seismic attack. The initial programme called for the testing of two walls, one without confinement and the other with mortar bed confining plates. Testing of masonry prisms[10] had indicated that inserting 3.1 mm thick confining plates in the mortar beds inhibited the formation of vertical splitting, increased the effective ultimate compression strain from 0.25% to at least 0.8%, and greatly reduced the slope of the falling-branch portion of the stress-strain curve. Theoretical ductility capacity of confined walls was shown[11] to be at least three times that for corresponding unconfined walls.

The two initial walls were heavily reinforced for flexure and with a reasonably high axial load, to ensure requirements of the draft code[9] were violated. Bars were lapped in the plastic hinge zone. Subsequent to the completion of the first two walls it was decided to test a third wall with lower axial load and a longer lap length for vertical reinforcement.

DESIGN OF TEST WALLS:

Wall Dimensions -

The size of the masonry shear walls was limited by the available clear height within the structural testing laboratory, and by the 500 kN capacity of the jack to be used for horizontal load application. Within these confines, the walls were chosen to have a high effective aspect ratio, and detailed to violate the slenderness regulations of the draft concrete and masonry design codes.

Maximum height of load application above the strong floor was restricted to 6.3 m. Since this is less than a typical three-storey wall height, wall width would not normally be subject to the special slenderness provisions within the plastic hinge zone. To create a critical situation, the walls were constructed from 140 mm wide concrete masonry units, and considered to be 0.737 scale models of walls with 190 mm blockwork. Thus a typical full-size storey height of 2.8 m could be modelled by 2.06 m. With a 300 mm allowance for a foundation beam this still resulted in

a useful wall height, at 6.0 m, slightly less than three storeys. However, in terms of slenderness and stability of the compression zone, the critical aspects of the wall dimensions will be the slenderness ratio over the lowest storey, and the moment gradient over the same region. Consequently the total wall height was divided into unequal storey heights of 2.1 m, 2.0 m and 1.9 m. Since horizontal load was applied by a single jack at the top of the wall, the moment gradient over the bottom storey was more gradual (i.e. close to constant moment) than would occur in a normal three storey wall, where horizontal inertia forces are generated at each floor level. In a regular multistorey structure with equal floor and roof masses, the centre of seismic force (assuming the linear code distribution of seismic loads) is at approximately 2/3 the wall height. Thus, inverting this figure, the test-wall height of 6.0 m is equivalent to a multi-storey wall 9.0 m, or 4.3 storeys high. The slenderness requirements of the draft design codes must therefore be considered. The wall length of 2.4 m resulted in an effective aspect ratio of 2.5. In terms of the equivalent 9.0 m multistorey wall with distributed lateral load, this translates to a prototype aspect ratio of 3.75.

Reinforced floor slabs 200 mm deep x 1200 mm wide were cast at first and second floor levels, and a 540 x 450 mm reinforced bond beam was placed at the top to distribute horizontal load, and anchor flexural reinforcement. Fig. 1 shows details of wall dimensions and reinforcement.

Wall Reinforcement -

All three walls were reinforced in similar fashion. Vertical reinforcement consisted of 12-DH16 (D = deformed; H denotes high strength grade : f_y = 380 MPa nominal; 16 indicates bar diameter in mm) bars over the potential plastic hinge region, decreasing in two steps to 6-DH16 bars over the top storey. The steel was lapped to starter bars from the foundation beam, and immediately above each floor level, with the lap length being 1000 mm (62.5 d_b) for Walls 1 and 2, and 1300 mm (81.3 d_b) for Wall 3. The increased lap length for Wall 3 was based on observed bond breakdown of lapped flexural reinforcement at the ends of the wall in Wall 1, and reflected an increased lap length requirement within plastic hinge zones agreed to by the drafting committee of the masonry design code between times of constructing Walls 1 and 3.

The 16 mm diameter bars used for vertical reinforcement are the largest size allowed for nominal 140 mm masonry blockwork[9], and as each wall was reinforced, with one bar per cell, the walls can be considered to contain the maximum feasible level of flexural reinforcement. However, as the steel ratio, based on gross wall section dimensions was ρ = 0.00718, the walls were comparatively lightly reinforced by reinforced concrete standards.

Shear reinforcement consisted of D12 (nominal f_y = 275 MPa) bars at 200 mm centres throughout the wall height, except at floor slab level.

Confining Plates

Wall 2 differed from the basic design of Wall 1 only in that the plastic hinge zone at the wall base contained 600 mm long stainless steel confining plates at each end of the wall within the second to eighth mortar courses. No confining plates were placed in the bottom mortar course (i.e. between foundation beam and bottom layer of blocks) as it was felt that the foundation beam would provide adequate confinement. The confining plates were cut from 3.1 mm thick type 304 stainless steel, and followed the net dimensions of the blockwork, including cross webs, with a 5 mm clearance to outside dimensions of the wall to allow for pointing. Fig. 2 shows a confining plate placed in a mortar bed during construction.

Walls 1 and 3 did not include confining plates.

Axial Load Level

Walls 1 and 2 were tested with an axial load of 556 kN applied to the top of the wall. Together with the wall weight of 84 kN, this resulted in an axial load of N_u = 640 kN at the wall base, corresponding to an axial stress of 1.90 MPa. This was considered to be a reasonable upper level of axial load occurring in practice. Wall 3 had a reduced axial load of 166 kN applied, resulting in a total load of N_u = 250 kN at the wall base, corresponding to an axial stress of 0.744 MPa. This is about the minimum axial stress level that can be expected from a four storey wall of 190 mm blockwork supporting a tributory floor width of 6 m at each floor and roof level.

WALL CONSTRUCTION:

The walls were laid up by a professional mason, on reinforced concrete foundation beams bolted to a strong floor. Open-end bond beam blocks were used throughout the wall, except for end blocks, which were alternately 15.11 lintels (half blocks) or 15.13 deep lintels, as shown in Fig. 1. Use of open-end bond beam blocks is recommended by the draft masonry design code[9], and it results in a continuous latticework of grout throughout the wall, improving general integrity of construction.

Each storey-height was grouted in one operation by the high-lift grouting method using ready-mix grout of specified 28-day strength 17.5 MPa. Owing to lack of a small enough immersion vibrator, the walls were vibrated by rodding in each cell. Grout was placed in two lifts with full rodding of each lift, but without reconsolidation after a settling period. Despite the less than ideal vibration provided, no significant settlement was noted, and condition of the grout core, when examined after completion of testing the walls, was good.

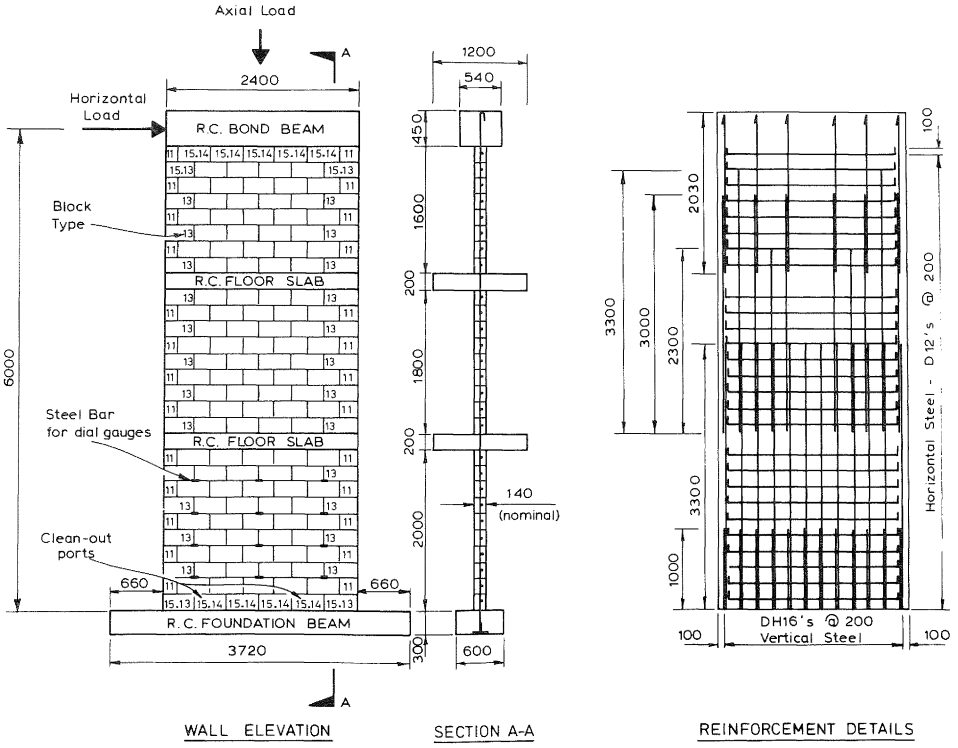

FIGURE 1 - WALL DIMENSIONS AND REINFORCING

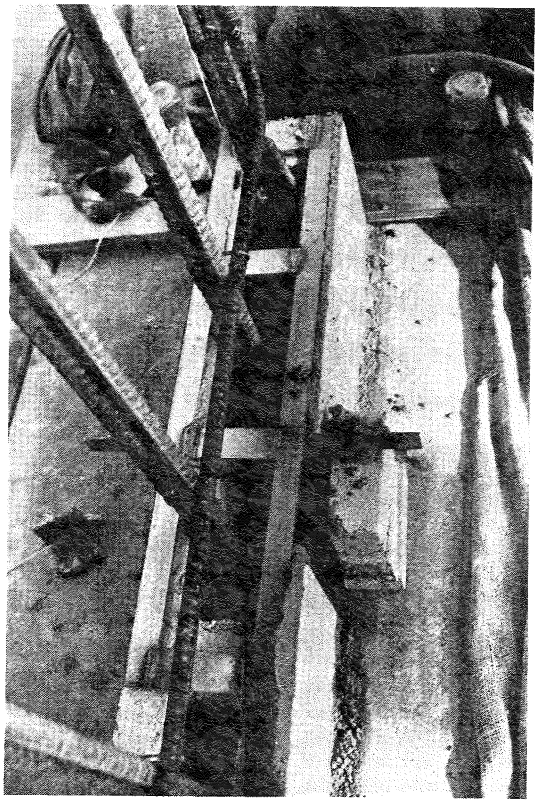

FIGURE 2 - CONFINING PLATE IN MORTAR BED OF WALL 2

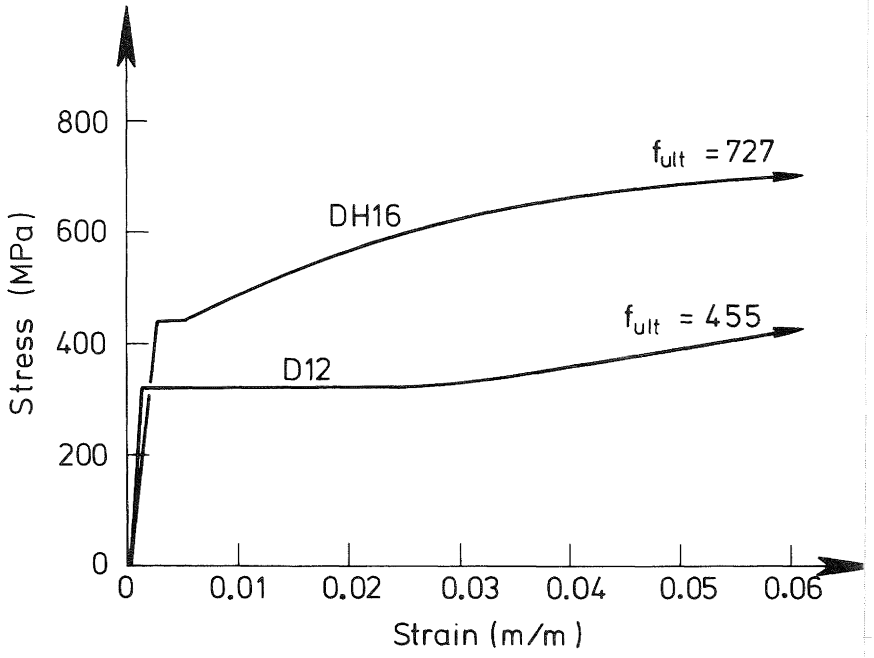

FIGURE 3 - STRESS-STRAIN CURVES FOR WALL REINFORCEMENT

Confining steel plates for Wall 2 were laid without significant protest by the mason during normal block laying. Once he had obtained some experience with the thickness of mortar bed required on each side of the plates, no problems were experienced in inserting the plates, and it was not possible after completion of construction to visually detect the presence of the plates.

MATERIAL PROPERTIES:

Material properties for the three walls are summarised in Table 1. Grout and mortar strengths were obtained from standard compression tests on 200 mm x 100 mm cylinders taken from the material during construction of the bottom storey of each wall, and are the average of at least three cylinders in each case. Grout and mortar strengths for second and third storeys have not been listed as they were not particularly relevant to the strength or stiffness of the walls, but were similar to the values listed for the first storey.

It will be noted that mortar strength was consistently lower than the code specified minimum of 12 MPa. Results of prism tests[10], which also contained substandard mortar indicate that the low mortar strength was not critical in terms of masonry compression strength.

Grout for Wall 1 was obtained from a different Ready-mix concrete supplier than for Walls 2 and 3, and has a significantly lower compression strength, though grout for all walls exceeded the minimum specified strength of 17.5 MPa. Results of the wall tests, reported later indicate that this variation, particularly between Walls 1 and 2, did not have a great effect on wall performance in that elastic deflection behaviour and neutral axis position at ultimate for these two walls were very similar. It thus appears that the strength difference indicated by tests on cylinders formed in steel moulds did not occur in the walls, presumably because excess water was absorbed from the weaker Wall 1 grout by the blockwork, reducing its water : cement ratio, and increasing its strength in-situ.

DH16 vertical reinforcement for all three walls came from a single batch, as did the D12 horizontal reinforcement. Stress-strain curves from tensile testing of three samples of each size are plotted in Fig. 3. It will be noted that the DH16 steel has a very short yield plateau, with strain-hardening setting in at a strain of 0.55%.

Samples cut from the stainless steel used for the confining plates of Wall 2 exhibited very ductile behaviour without a discernable yield strength. Ultimate elongation was 64%, and stress at a strain of 0.5%, and at ultimate were 316 MPa and 649 MPa respectively.

LOAD APPLICATION:

Horizontal load was applied by a double-acting 500 kN capacity M.T.S. hydraulic actuator at the centre-height of the bond beam (see Fig. 1) and reacted against a specially constructed reaction frame bolted to the strong floor. Gimbels were provided between the jack and reaction frame, and between jack and bond beam, to allow free rotation of the jack in the vertical plane, thus accommodating expected vertical movements of the wall ends under lateral load. The front gimbel was tensioned to the far end of the bond beam by two 32 mm Macalloy rods passing through preformed ducts and anchored against a steel plate.

Vertical load was applied to the top of the bond beam by four 300 kN capacity centre-hole hydraulic jacks manifolded together to a single pumping unit to ensure equal load at all times. The jacks reached against horizontal strong-backs straddling the wall, and were individually tied to the strong-floor by 25 mm dia. high strength steel tie rods.

To simulate the behaviour of a wall

TABLE 1 - WALL DETAILS AND MATERIAL STRENGTHS

	WALL 1	WALL 2	WALL 3
AXIAL LOAD*	640	640	250
S.S. CONFINING PLATES	No	Yes	No
BLOCK COMP. STRENGTH (MPa)	40.0	40.0	40.0
MORTAR COMP. STRENGTH (MPa)	10.9	8.4	8.4
GROUT COMP. STRENGTH (MPa)	21.1	35.3	29.0
VERTICAL REINFORCEMENT (DH16) f_y (MPa)	434	434	434
LAP LENGTH (mm)	1000	1000	1300
HORIZ. REINFORCEMENT (D12) f_y (MPa)	322	322	322

* At wall base. Includes self weight of walls.

within a building, it was necessary to provide lateral stability at each floor level, and at the level of load application, without impeding free movement in the plane of the wall. Stability was provided by transverse rollers, two on each side of the wall at each floor level, reacting against an R.H.S. frame guyed to the strong floor at each floor level by steel guy wires incorporating tensioning devices at ground level. The transverse rollers could be adjusted until just free from contact with the floor slabs, thus providing lateral stability on either side if the wall tended to move laterally.

For each wall horizontal load was applied in a series of cyclic load reversals of increasing displacement amplitude. Two initial cycles were applied in each direction at comparatively low displacements, with the second cycle being to the theoretical load at which yielding of the tension reinforcement furthest from the neutral axis first occurred. These cycles were used to investigate elastic response and to determine the experimental 'yield' displacement Δ_y which was found graphically by extrapolating a straight line from zero through the load-displacement point at first yield, measured at the height of load application, to the theoretical ultimate flexural capacity based on an ultimate compression strain of 0.003, and measured material strengths. No allowance for strain hardening was made in assessing theoretical flexural strength, and no strength reduction factor was employed. Δ_y was taken as the average of the displacements so calculated for the two directions of loading.

Subsequent testing consisted of at least three complete cycles to each of successive displacement ductility factors (i.e. multiples of Δ_y) of approximately μ = 1.5, 3, 4.5 and 6, unless premature failure occurred.

INSTRUMENTATION:

Loads -

Horizontal load was monitored by a strain gauged load cell in series with the actuator ram with a reading sensitivity of approximately 0.1 kN, and a repeatability of better than 0.5kN.

The jacks and pressure system used for vertical load application were calibrated in parallel in a 10 MN capacity DARTEC Universal Testing Machine, with load in the jacks being indicated by pressure in a precision pressure gauge. This gauge was used to set and monitor applied vertical load during testing. It is expected that the accuracy of vertical load application was about $\pm$ 2%.

Lateral Displacements -

In-plane horizontal displacements at the base, first and second floors, and at the level of load applications were monitored by 200 mm travel SAKAE linear potentiometers mounted on an RHS support frame. Out-of-place displacements were checked periodically with a theodolite, and were found to be less than $\pm$ 2.5 mm at all stages of loading.

Vertical Strains -

Vertical strains in the masonry were measured over sequential 400 mm gauge lengths on vertical lines up the wall centre line and lines 400 mm from each edge of the wall by 50 x 0.01 mm travel Mitutoyo dial gauges mounted on both sides of the wall, on bars passing through mortar beds at 400 mm centres. Averaging the displacements on either side of the wall and dividing by the gauge length provided the average strain. Gauge lengths were provided continuously between wall base and first floor level, but were not included in the second or third storeys. By plotting strain distributions along the wall at a given elevation, curvature distributions could be obtained. A slight modification to the arrangement of vertical dial gauges was made for Walls 2 and 3, where the gauge length immediately adjacent to the wall base was reduced to 200 mm (i.e. one block height) to better measure the local curvature at the wall base.

Readings of load, displacement and strain were recorded manually, and a continuous plot of horizontal load against displacement at height of load application was obtained with an X-Y recorder.

More complete details of wall construction, testing and instrumentation are available in ref. 10. Fig. 4 shows a wall under test.

RESULTS:

Description of Wall Behaviour -

Wall 1:- Axial Load = 640 kN, no confining plates.

During initial elastic cycling, horizontal flexural cracking developed at all mortar courses between the base and the first floor of the wall. As the displacement was increased to the inelastic range it became evident that the lapped vertical reinforcement was modifying behaviour within the plastic hinge region, by keeping the centre portion of the lap elastic as a result of the increased flexural strength. For example, at a ductility of μ = 2.5, maximum crack widths at the second, third and fourth mortar courses were less than 0.2 mm, while the base crack was 4.8 mm wide, and the width of cracks at courses 5, 6 and 7 (top of lap and above) were each greater than 1.5 mm.

Inclined flexure-shear cracking down vertical header joints and diagonally through blockwork was first noticed at an average shear stress, based on gross cross-section dimensions of 0.71 MPa.

During cycling to μ = 2.84, crushing of mortar beds and vertical splitting of blocks within the compression zones near the wall base was noted. The vertical splitting, which is characteristic of the failure mechanism of masonry in

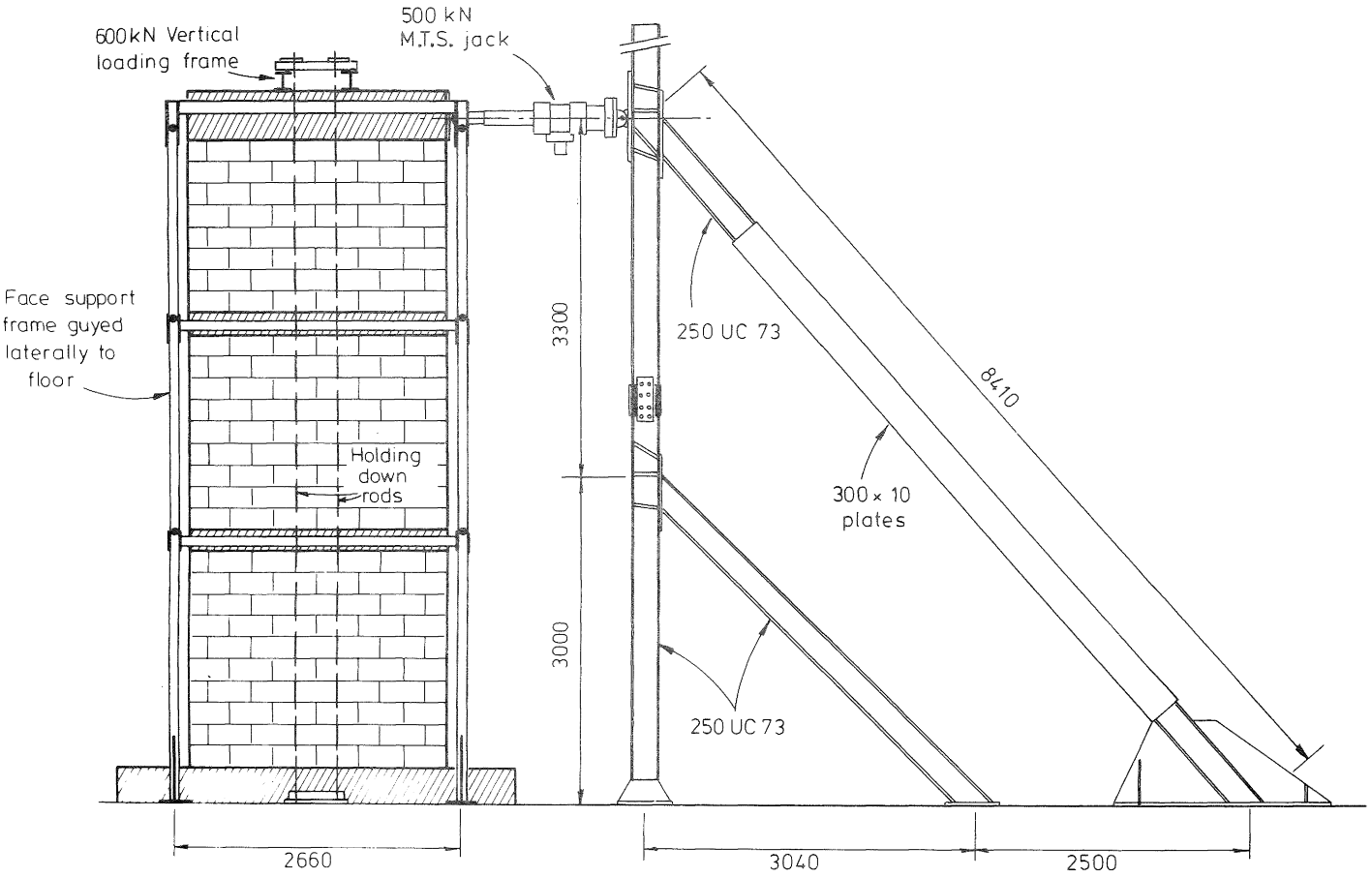

FIGURE 4 - TEST SET-UP

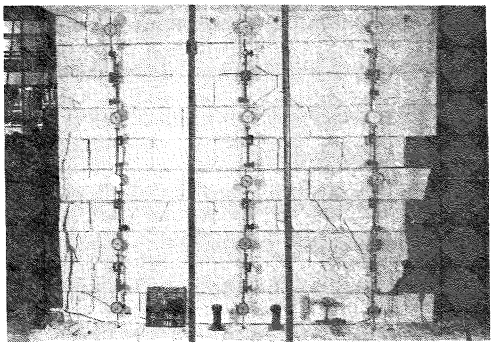

(a) After 3 cycles at μ = 2.84

(b) After 2 cycles at μ = 3.9

FIGURE 5 - WALL 1 CONDITION DURING TESTING

(N_u = 640 kN; No confining plates)

compression[12], resulted in bond failure along the extreme tension reinforcement on reversal of load direction. The combined effects of crushing and splitting of the compression zones, and bond failure at the tension end of the wall resulted in rapid degradation of load capacity at this level of ductility. Fig. 5a shows the condition of Wall 1 after three complete cycles to $\mu = 2.84$. Note the loss of face shells in compression zones, and the extensive vertical splitting of masonry.

Two further cycles were applied to ductility levels of approximately $\mu = 3.9$, the maximum that could be applied without reblocking the MTS actuator during each displacement half-cycle. Further degradation, both visually and in terms of load capacity occurred, and the testing was discontinued when ability of the wall to support the applied vertical load became suspect. Fig. 5b shows a detail of the wall condition at the end of the test. The bond-failure of the tensile reinforcement in the lap region, and the degradation of the grout core are clearly apparent.

Wall 2: Axial Load = 640 kN, confining plates 600 mm long in 2nd to 8th mortar bed each end of wall.

Up to displacement ductility factors of $\mu = 2.84$, Wall 2 was subjected to the identical regime of applied displacements as Wall 1, in order to be able to examine the influence of confining plates on the behaviour. In the initial stages of testing response was very close to that of Wall 1, with Wall 2 being some 4% more flexible. Initial cracking was in the form of horizontal cracks at all mortar beds in the lower storey, and inclined flexure-shear cracking was first noted at an average shear stress of 0.76 MPa. Again it was apparent that the lapped vertical reinforcement was keeping the centre portion of the lap elastic, with much higher crack widths being noted above the lap.

Four complete cycles were imposed at $\mu = 2.84$, one more than Wall 1 was subjected to. Despite this very little load or physical degradation occurred. Minor crushing of mortar joints at the compression end of the wall base was noted, and some minor splitting of the face shells 100 mm from the wall end occurred. The confining plates appeared to adequately control these cracks and inhibit them from spreading into adjacent blocks. Fig. 6a shows the condition of Wall 2 after four cycles to $\mu = 2.84$. Compare with the condition of Wall 1 (Fig. 5a) at the corresponding stage of testing.

Since severe degradation had not occurred at $\mu = 2.84$ there was little point in duplicating the final stages of testing of Wall 1. Instead, four additional cycles were imposed at a displacement ductility factor of $\mu = 4.26$, requiring reblocking of the actuator during each half cycle of loading. During cycling at this level, some cracking and crushing of individual face shells in the compression zones at the wall base occurred, and in the latter stages of testing, buckling of the extreme compression bar at the bottom course of blockwork occurred at both ends of the wall. Fig. 6b shows the general condition of Wall 2 at this stage of the test sequence. Comparison with Fig. 5a indicates that Wall 2 was in much better condition at this stage than was Wall 2 after only three cycles to the lower ductility of $\mu = 2.84$. Note that the damage does not extend into the second course, as a result of restraint provided by the confining plate.

The final stage of testing consisted of two cycles to $\mu = 5.68$. Extensive spalling of the face shells in the compression zones occurred, and bond failure was noted at the extreme tension bar at one end of the wall. Fig. 6c shows general condition of Wall 2 at end of test, and Fig. 6d shows a detail of one wall end after removal of loose face shells which had separated from the grout core, but which were not dislodged during testing. Damage to the grout core over the bottom two courses is apparent in Fig. 6d, but the confining plates have minimised the damage. Compare with the condition of Wall 1 at end of test (Fig. 5b). It is felt that Wall 2 could have been successfully repaired after completion of testing.

Wall 3: Axial Load = 250 kN, no confining plates, increased lap length (1300 mm)

Initial stages of response of Wall 3 were similar to the previous two walls. Inclined flexure-shear cracking occurred at an average shear stress of 0.67 MPa, somewhat lower than for Walls 1 and 2, but because of the lower flexural capacity of Wall 3, this corresponded to a higher level of ductility ($\mu = 1.6$ compared with $\mu = 1.0$ for Walls 1 and 2).

Vertical splitting in the compression zone was first noticed at $\mu = 2.8$ as the displacement was being increased to the first peak of four cycles to $\mu = 3.2$. At peak displacement, crushing at several mortar courses in the compression zone was noted. Considerable vertical splitting occurred during subsequent cycles to $\mu = 3.2$, mainly confined to the bottom three blocks, though as shown by Fig. 7a, significant damage has resulted at the level of the top of the lap. Clearly the crushing strain has been exceeded by this stage of testing. Again the lapped vertical reinforcement kept the centre portion of the lap region elastic.

During the first of four cycles to $\mu = 4.8$, substantial extension to vertical splitting occurred, with face shells falling off the compression end of the wall. The physical degradation increased with subsequent cycles, and bond failure along the extreme tension bar at one end of the wall occurred at an early stage of cycling to $\mu = 4.8$.

The final stage of testing consisted of two cycles to $\mu = 6.4$. Degradation was rapid and extensive with crushing and collapse of the grout core where the face shells had previously separated. Fig. 7b shows the wall condition at the end of test, with loose rubble removed

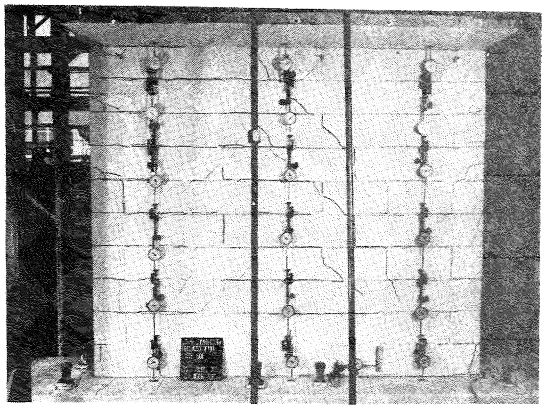

(a) After 4 cycles at μ = 2.84

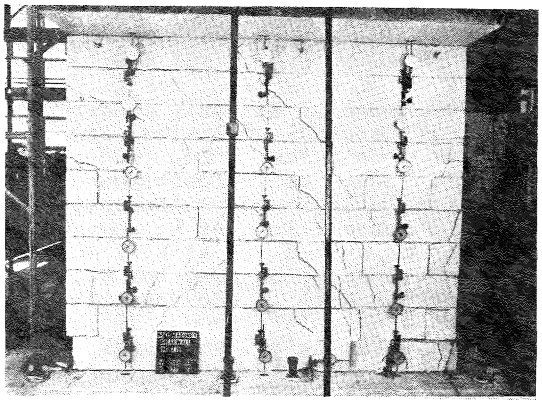

(b) After 4 cycles at μ = 4.26

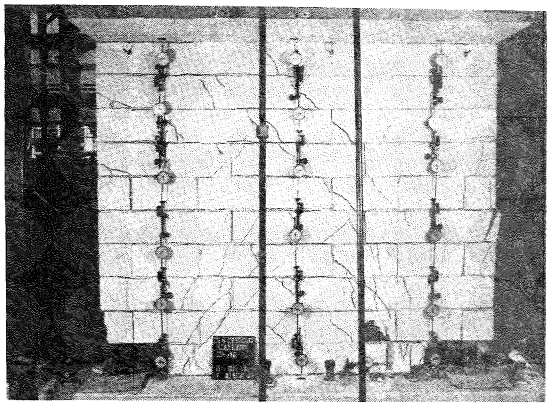

(c) After 2 cycles at μ = 5.68

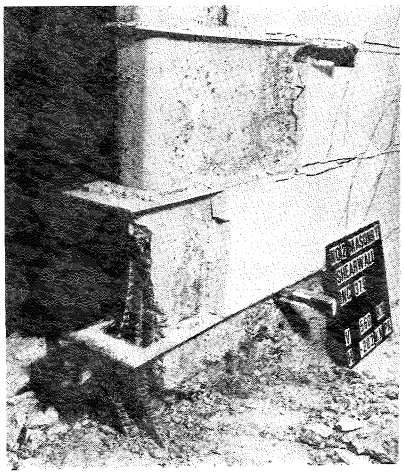

(d) After 2 cycles to μ = 5.68 (Detail)

FIGURE 6 - WALL 2 CONDITION DURING TESTING

(N_u = 640 kN; Confining plates at wall base)

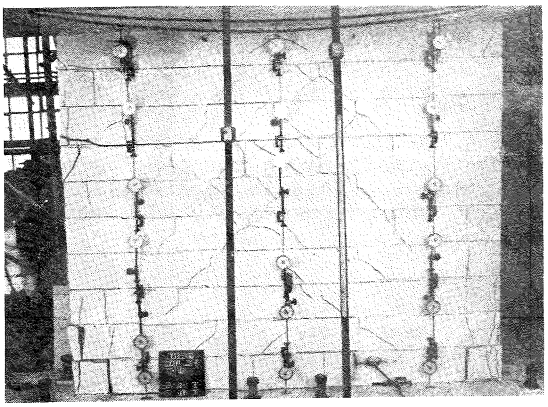

(a) After 4 cycles at μ = 3.2

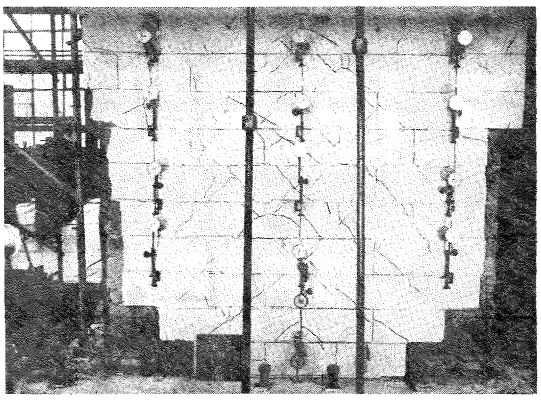

(b) After 2 cycles at μ = 6.4

FIGURE 7 - WALL 3 CONDITION DURING TESTING

(N_u = 250 kN; No confining plates)

from the bottom of the wall. The complete failure of the compression zones is apparent.

It was noted that bond failure occurred only at the extreme tension bar at one end of thewall, and only occurred as a result of vertical splitting from high compression strains. Consequently it is believed that the increased bond length materially improved performance of Wall 3. However, it must be remembered that as a result of reduced axial load, the extent of compression zone for Wall 3 was less than for Wall 1, and thus the extent of vertical splitting was reduced. Bond conditions for Wall 3 were thus probably more advantageous particularly at late stages of testing than for Wall 1.

Load-Deflection Behaviour

Load deflection hysteresis loops for the three walls are shown in Figs. 8 to 10 respectively. Included on the plots are lines showing the theoretical ultimate lateral load, based on conventional ultimate strength theory for reinforced concrete, using measured material properties, without incorporating a strength reduction factor. The masonry compression strength was taken as f'_m = 25 MPa, an average value found from prism tests on 140 mm masonry prisms made with similar constituents to the wall, as part of the test programme[10]. Also included on the plot is the load at which the extreme tension reinforcement at the wall base first reaches yield. In all cases deflections in Figs. 8 to 10 were measured at the level of the applied load.

Wall 1

Fig. 8 shows that very good behaviour was obtained for cycles up to μ = 1.42. At this level of ductility, first peak loads in each direction are only 2-3% below theoretical ultimate lateral load, and degradation of peak load in the subsequent two cycles is comparatively minor.

During the first half cycle to μ = 2.84 the peak load rises quickly above the theoretical ultimate capacity to a maximum of 323 kN, as a result of the very short yield plateau of the flexural DH16 reinforcement and consequent early strain hardening. On load reversal, the drop in load capacity resulting from bond slip just before reaching μ = 2.84 is clearly apparent. Strength and stiffness degradation over the subsequent two cycles are very marked, and peak loads on the 3rd cycle, at 205 kN and -220 kN average 66% of the initial peak. Although this level of load degradation is higher than would normally be considered satisfactory for major seismic resisting elements, it should be noted that the strength reduction factor associated with flexural design of this wall would be approximately ϕ = 0.70. Thus after three cycles of loading to μ = 2.84, strength has only just degraded to the design value.

However, in view of the subsequent rapid degradation at μ = 3.9, it is clear that μ = 2.84 should be considered as an upper limit on available ductility for this wall. Because of the degree of damage sustained at this stage it is not felt that the wall could have been successfully reinstated by current repair techniques without changing the structural configuration of the ground floor level.

Earlier tests on squat walls indicated that sliding of the entire wall on the base was a major form of stiffness degradation. No measurable base slip occurred with this wall. This is reflected in the lack of a 'soft' response at low loads, characteristic of base slip, in Fig. 8.

Wall 2

Fig. 9 shows the load-displacement hysteresis loops for Wall 2. Up to a ductility of μ = 1.42 behaviour is very similar to that for Wall 1, with Wall 2 showing slightly increased flexibility. This is despite the higher strength obtained from cylinder tests on grout for Wall 2 compared with Wall 1 values. It is felt that grout strength in-situ was much the same for the two walls, as a significantly higher value for Wall 2 should have resulted in higher modulus of elasticity, and hence increased stiffness of Wall 2, instead of the opposite trend actually observed.

At displacement ductilities of μ = 2.84, Wall 2 exhibited extremely stable hysteresis loops, with all four peak loads in each direction exceeding the theoretical ultimate. Behaviour is markedly better than for Wall 1 despite the extra cycle at μ = 2.84 applied to Wall 2.

Cycling at μ = 4.26 resulted in significant strength degradation as a result of damage to end compression blocks, and buckling of compression steel. However, initial cycles exceeded theoretical ultimate, and after four complete cycles, peak loads are still averaging 81% of theoretical ultimate. Thus satisfactory behaviour was obtained at this level of ductility.

Final cycles to a ductility factor of μ = 5.68 reflect the effects of bond-failure on the end tension bar, compression zone collapse, and buckling of the extreme compression reinforcement. However, degradation is comparatively slow, and similar to that experienced by Wall 1 at half this ductility.

As with Wall 1, there was no sliding of the wall along the base at any stage of testing. This is apparent in Fig. 9 from the comparatively high stiffness of the loops at low loads.

Wall 3

In the early stages of testing, Wall 3 was noticeably more flexible than Walls 1 and 2, as a result of the reduced axial load (see Fig. 10).

Hysteresis loops at μ = 1.6 reveal significant degradation of stiffness in one direction only. This is reflected in reduced peak loads in the 'push' direction, but on loading to μ = 3.2, the maximum load attained is the maximum

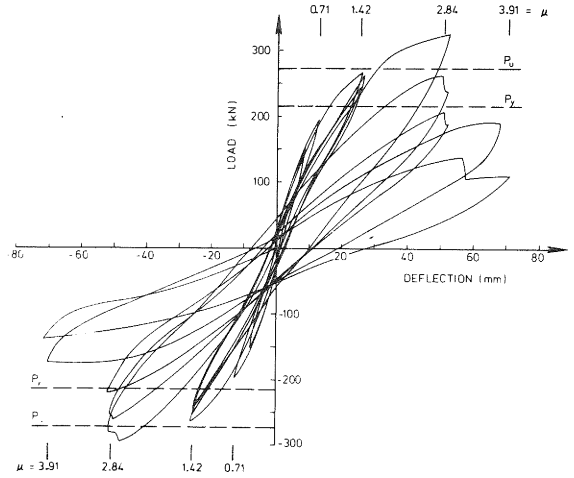

FIGURE 8 - WALL 1 LOAD-DEFLECTION HYSTERESIS LOOPS
(N_u = 640; No confining plates)

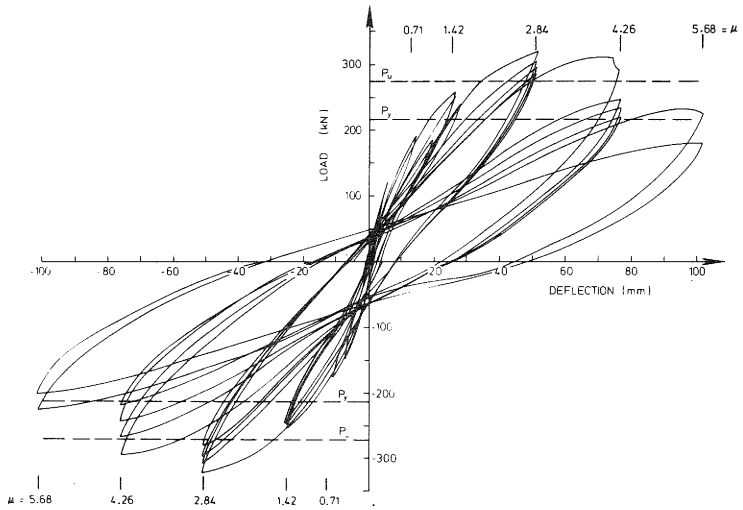

FIGURE 9 - WALL 2 LOAD-DEFLECTION HYSTERESIS LOOPS
(N_u = 640 kN; Confining plates at wall base)

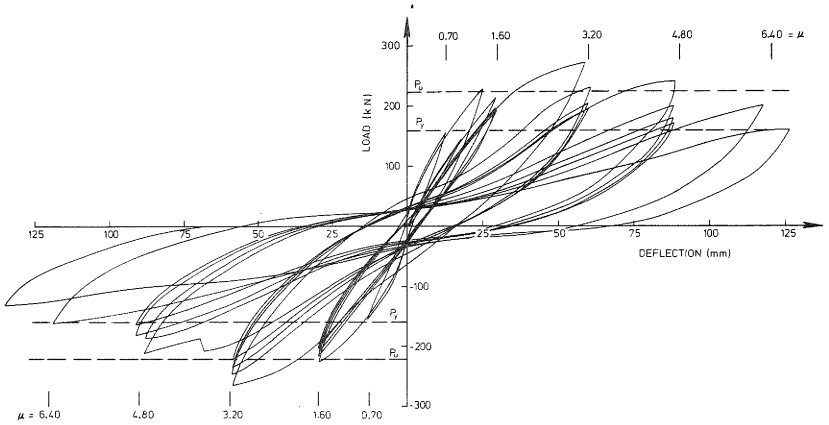

FIGURE 10 - WALL 3 LOAD-DEFLECTION HYSTERESIS LOOPS
(N_u = 250 kN; No confining plates)

for the whole test sequence. It is thus clear that no permanent load degradation had occurred at $\mu = 1.6$.

Despite the structural damage in the form of crushing and vertical splitting of end blocks at $\mu = 3.2$ described earlier, and shown in Fig. 7a, degradation of hysteresis loops in Fig. 10 is not severe, with peak loads after four cycles to $\mu = 3.2$ being $0.90\ P_u$ and $1.0\ P_u$ in the two directions of loading. The lack of significant degradation is probably a result of the short compression zone, the absence of bond failure, and the compensating effects of strain-hardening of the tension reinforcement.

At $\mu = 4.8$, degradation was comparatively rapid, partly as a result of bond failure on the extreme tension bar in the reversed loading (pull) direction. Note the pronounced load drop at - 68 mm displacement on the first cycle to $\mu = 4.8$. Nevertheless, after four cycles to $\mu = 4.8$, peak loads are still about $0.72\ P_u$. This is somewhat less than the design ultimate strength of $0.79\ P_u$, where 0.79 is the strength reduction factor appropriate to the axial load ratio $N_u/f'_m Ag = 0.03$.

At $\mu = 6.4$ degradation is extensive, and peak loads drop rapidly to about 50% of P_u.

The hysteresis loops exhibit some softening of the response at low loads, particularly for ductilities of $\mu = 3.2$ and higher. This softened response is characteristic of shear deformation, particularly as a result of sliding of the wall as an entire unit along the base. However, measurements of base slip indicated that this contributed less than 5% to total deformation of Wall 3.

Fig. 10 illustrates that if bond failure can be avoided, degradation of walls with light axial load may be comparatively gradual, despite crushing of compression zones.

Vertical Strains

Space limitations do not permit the presentation of full information from the vertical strains measured by dial gauges on both sidesofeach wall. Complete data are available in reference 10.

For illustrative purposes, profiles of vertical strain at different selected elevations for Walls 1 and 2 are shown in Figs. 11 and 12. Strains calculated from the average of the readings at corresponding positions on the two sides of the wall have been plotted at the appropriate position on an elevation of the wall length, and the best-fit straight line has been drawn through the three such data points at each level. Profiles plotted for different ductility levels in each case represent condition on the first peak displacement in each direction to the particular ductility factor. In all cases the strain profiles indicate reasonably linear behaviour, and it is thus felt that extrapolation to the wall boundaries, as shown in the graphs, is justified. No strain profiles have been drawn for Wall 1 at $\mu = 3.9$ as gauge readings at this stage of loading had become unreliable as a result of spalling of face shells and damage to the grout core at the lower gauge locations. The vertical reinforcement yield strain of $\varepsilon_y = 0.0025$ has been plotted on each profile for comparative purposes.

The most significant point illustrated by Figs. 11 and 12 is the great reduction in strains occurring at sections close to the midheight of the laps (Figs. 11b and 12b) compared with values at the wall base or immediately above the lap. This remains the case in Wall 1 even after bond failure at the extreme tension reinforcement.

Figs. 11c and 12c show that very high tensile strains existed at the wall base, and that much of the reinforcement exceeds the strain at onset of strain-hardening of 0.5%.

Compression strains at $\mu = 2.84$ adjacent to the wall base in Wall 1 are a maximum of 0.23% and 0.32% in the two directions of loading respectively. As crushing and vertical splitting occurred during these initial stages of loading to $\mu = 2.84$ it would appear that the recently proposed ultimate compression strain of 0.0025 is a reasonable value for high strength concrete masonry. Strain recordings on the other two walls also confirmed this, with no significant crushing or vertical splitting being noted at strains below 0.22%, but extensive damage being noted at strains as low as 0.28%. For Wall 2 (Fig. 12) extreme fibre compressive strains at $\mu = 4.26$ exceed the recommended unconfined strain of 0.25% for the bottom 1200 mm of the wall. It would thus seem that the extent of confinement for Wall 2, at 1400 mm above the base, was about right.

Maximum compression strains at the base of Wall 2 are in the vicinity of 0.5% at $\mu = 2.84$, 1.29% at $\mu = 4.26$, and 4.0% at $\mu = 5.68$. These are substantially higher than expected, and would indicate a shorter plastic hinge length than the theoretical value of $0.5\ L_w$.

The profiles of vertical strain shown in Figs. 11 and 12 also enable neutral axis positions to be estimated from intersection of the strain profiles with the zero strain axis. From comparison of Figs. 11c and 12c, it will be seen that neutral axis positions for the two walls at early stages of testing are very similar.

Between $\mu = 0.71$ and $\mu = 2.84$ the values for Wall 2 with Wall 1 values in parenthesis are: $\mu = 71$: c = 840 mm (860 mm), $\mu = 1.42$: c = 660 mm (610 mm), $\mu = 2.84$: c = 495 mm (440 mm). This again confirms that the compression strength of the masonry in the two walls is very similar, despite the significant difference in grout strength measured from steel-moulded cylinders.

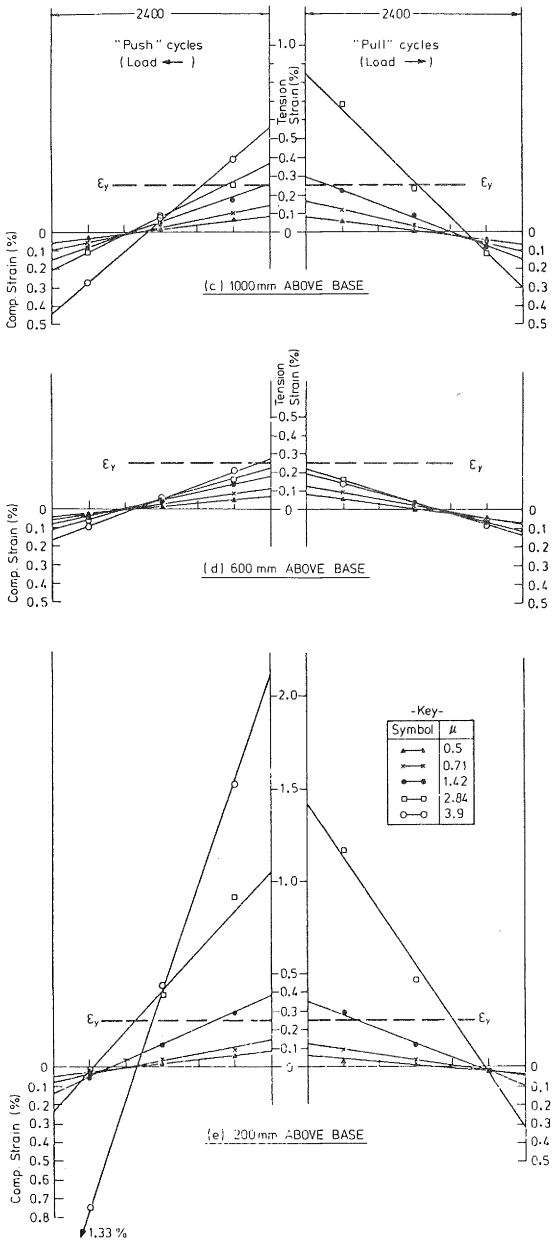

FIGURE 11 - WALL 1 STRAIN PROFILES AT DIFFERENT ELEVATIONS
(N_u = 640 kN; No confining plates)

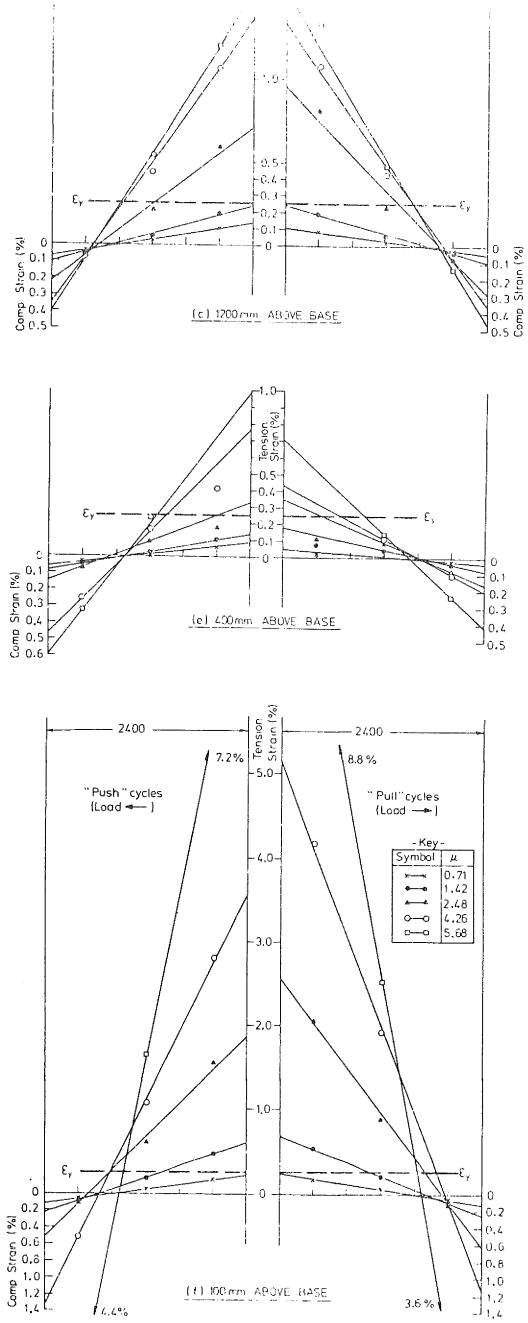

FIGURE 12 - WALL 2 STRAIN PROFILES AT DIFFERENT ELEVATIONS
(N_u = 640 kN; Confining plates at wall base)

Curvature Distributions and Plastic Hinge Lengths

Curvature distributions up the lower storey of each wall are plotted for peak ductilities in the two directions of loading in Figs. 13 to 15. Values calculated from the slope of the strain distributions (e.g. Figs. 11 and 12) have been plotted at the centre height of the appropriate gauge lengths, joined by straight lines and extrapolated linearly to the wall base. Note the different curvature scales used for Walls 2 and 3 compared with Wall 1.

In all cases the influence of the increased reinforcement ratio within the lap region is clearly apparent, with greatly reduced curvatures towards the mid region of the laps. There appears to be a more intense concentration of curvature close to the wall base in Walls 2 and 3 than in Wall 1. This can partly be explained by the shorter gauge length at the wall base for Walls 2 and 3, but comparison of interpolated curvatures at height 200 mm for Wall 2 with readings for Wall 1 indicates that a substantial discrepancy (about 30%) would still result. It appears that the discrepancy is a result of the spread of vertical cracking and bond failure up Wall 1 at a comparatively early stage of testing.

The curvature distributions of Figs. 13-15 enable an estimate of the equivalent plastic hinge length, L_p, to be made using the expression:

$$\Delta_p = \psi_p L_p (H - L_p/2) \qquad (2)$$

where

Δ_p = plastic displacement = $\Delta - \Delta_e$

ψ_p = plastic curvature at the wall base = $\psi - \psi_e$

H = height of wall

and Δ_e and ψ_e are the elastic displacements and base curvatures corresponding to the level of applied load.

On the basis of this approach, equivalent plastic hinge lengths were as follows:

Wall 1, at $\mu = 2.84$: $L_p = 0.34\ L_w$

Wall 2, at $\mu = 4.26$: $L_p = 0.16\ L_w$

Wall 3, at $\mu = 4.8$: $L_p = 0.12\ L_w$

These values are very low in comparison with the value of $L_p = 0.5L_w$ adopted in design charts for ductility capacity[7,11]. This very short equivalent plastic hinge length is presumably a result of the stiffened lap region concentrating plastic deformation over a small region at the wall base. The consequences are a rapid increase in peak compression strain at the wall base with ductility, and a reduced available ductility capacity compared with values predicted on the basis of $L_p = 0.5\ L_w$.

It should also be noted that there was a clear tendency with both Walls 2 and 3 for the plastic hinge length to decrease substantially as the ductility factor increased.

DISCUSSION OF RESULTS:

Comparison between theoretical and experimental behaviour of the three walls are summarised in Table 2.

Flexural Strength

Ultimate flexural strength of all three walls was close to 1.20 times ideal theoretical capacity based on normal assumptions for ultimate strength of reinforced concrete and measured material strengths. In all cases maximum over-strength occurred at comparatively low ductility factors ($\mu < 3$) as a result of strain hardening of the flexural reinforcement at comparatively low strains.

It should be noted that the actual flexural strengths are 80% higher than ideal strength based on $f'_m = 8$ MPa and $f_y = 380$ MPa, for Walls 1 and 2, and 65% higher than ideal strength for Wall 3. This potentially very large flexural overstrength for walls designed to code default strength values should be considered when adopting a capacity design approach for required shear strength.

Shear Strength

Inclined shear cracking developed at approximately 0.70 MPa average shear stress based on the gross cross section, with a slight dependence on axial load apparent: Wall 3 with low axial load cracking slightly earlier than Walls 1 and 2.

Shear capacity of the walls was assessed in accordance with the code approach[9] which requires all shear force in potential plastic hinge zones to be carried by reinforcement. Assuming an effective depth for the distributed flexural reinforcement of $0.8L_w$, the ideal shear capacity, based on the measured yield strength of the horizontal reinforcement (322 MPa) is thus

$$V_u = \frac{A_v . f_y\ (0.8L_w)}{s}$$

$$= \frac{113 \times 322 \times (0.8 \times 2.4)}{0.2} \quad N$$

$$= 349\ kN$$

Walls 1 and 2 attained maximum shear forces of $0.92\ V_u$ and $0.93\ V_u$ respectively, with an average maximum shear stress (gross section area) of 0.97 MPa.

Despite the high stress level, no yield of shear reinforcement occurred, and thus current design methods for shear may be considered adequately conservative.

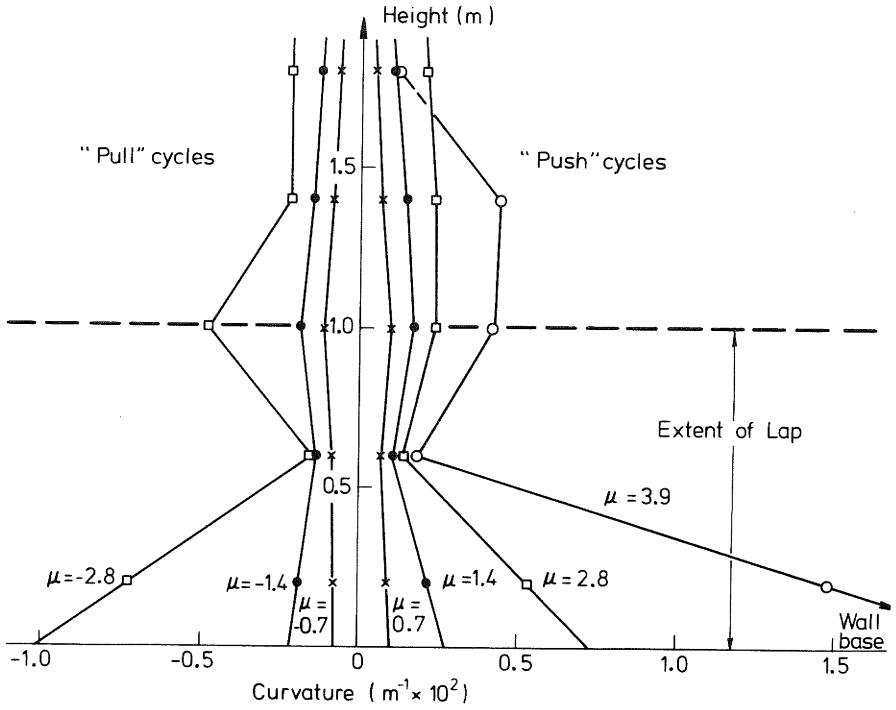

FIGURE 13 - WALL 1 CURVATURE PROFILES AT PEAK DUCTILITIES

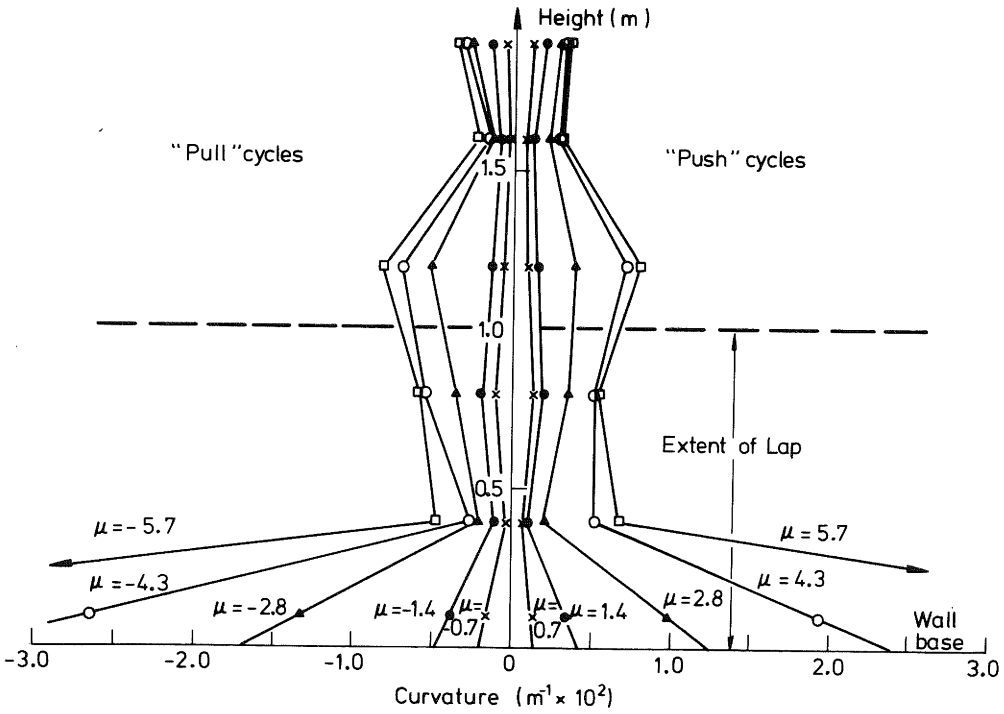

FIGURE 14 - WALL 2 CURVATURE PROFILES AT PEAK DUCTILITIES

Elastic Deflections

Table 2 includes a comparison of theoretical and experimental yield displacements. Two methods have been used to predict yield displacement. The code approach[9] utilises the gross section area for flexural and shear deformations, but uses an artificially low effective modulus of elasticity of 6 GPa. Deflections predicted by this approach are about 25% high for Walls 1 and 2, and 1% low for Wall 3. The elastic theory approach requires a cracked-section analysis, and the calculation and integration of the curvature distribution up the wall for the load when first yield occurs at the wall base. The displacement so found is factored by the ratio of theoretical ultimate load to theoretical first-yield load to obtain the 'yield' displacement. The lower value in the range shown in Table 2 includes the stiffening effect of the lapped reinforcement at the wall base, assuming perfect bond, while the higher value ignores the increased reinforcement ratio within the lap region. Neither figure includes a shear deflection term. It will be seen that best agreement results from ignoring the effect of the lap, underestimating yield displacements by 8% for Walls 1 and 2, and 3% for Wall 3.

Available Ductility

Theoretical ductility capacity for the three walls was assessed using the design charts of references 7 and 11, and has been included in Table 2. Exact experimental values for ductility capacity are not possible because of large steps in ductility factor between successive levels of displacement cycling. The criterion adopted for assessing experimental ductility capacity has been an unacceptably high rate of strength degradation. For want of a better definition, the limit has been taken as the level of ductility at which cycling for four complete cycles decreases load capacity below the dependable strength, based on measured material properties. It should be noted that this definition of ductility differs from that adopted in developing the theoretical curves, which are based on a limiting ultimate strain.

For the two unconfined walls collapse of compression zones was initiated by crushing and vertical splitting which occurred at compression strains close to the proposed ultimate strain of $\varepsilon_u = 0.25\%$. For Wall 1, with high axial load, this resulted in rapid strength degradation at a ductility factor of $\mu = 2.8$, as vertical splitting resulted in bond failure at

TABLE 2 - SUMMARY OF WALL BEHAVIOUR

	WALL 1	WALL 2	WALL 3
Flexural Strength (kN)			
P_u Theor.	272	272	222
$P_{u.Exp.}$	323	326	268
$P_{u.exp}/P_{u.Theor.}$	1.19	1.20	1.21
Shear Strength $V_{u\ Th}$ (kN)	349	349	349
Yield Displacements (mm)			
$\Delta_{y\ exp}$	17.9	17.9	18.5
$\Delta_{y\ code}$	22.6	22.6	18.5
Δ_{y} El. Theory	12.1-16.5	12.1-16.5	13.1-18.1
Ductility			
Theoretical*	2.3	7.8	2.9
Experimental**	< 2.8	> 4.3	< 4.8

* Based on limiting ultimate strain
** Based on limiting load degradation

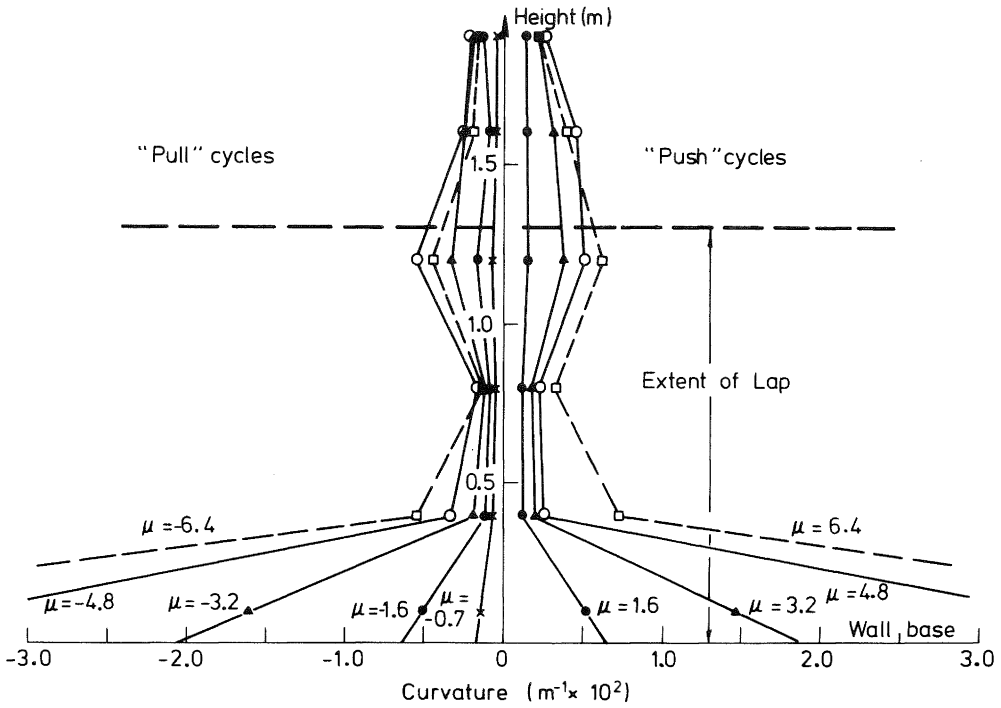

FIGURE 15 - WALL 3 CURVATURE PROFILES AT PEAK DUCTILITIES

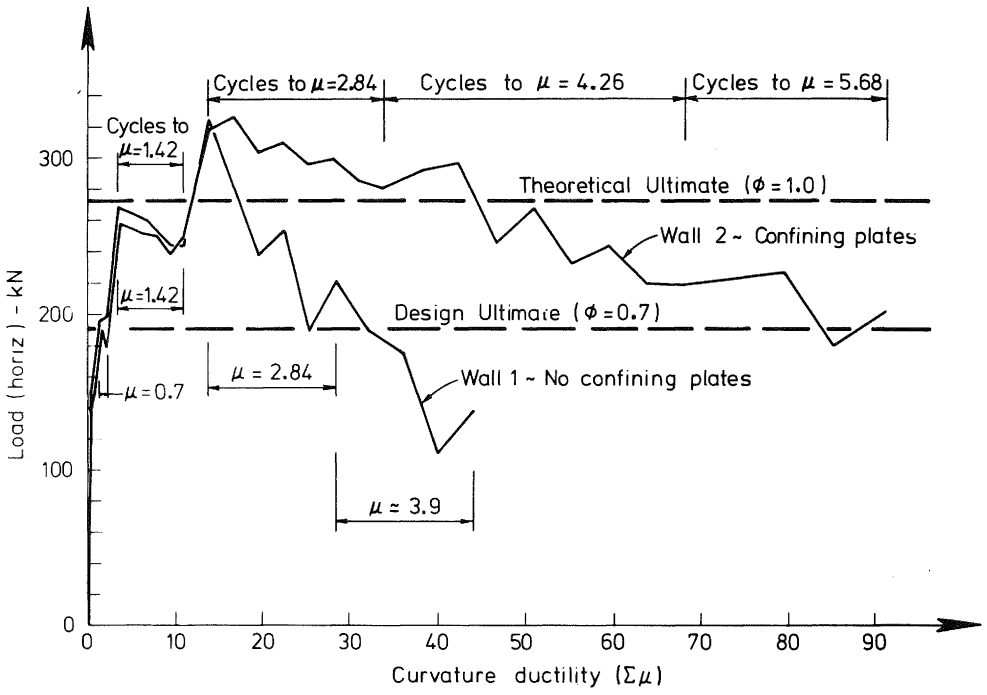

FIGURE 16 - CUMULATIVE DUCTILITY DEMAND, WALLS 1 AND 2

the laps of tension reinforcement at each end of the wall. Consequently this is taken as an upper limit to available ductility for this wall. Wall 3 had a lower axial load and a longer splice length of starterbars. Vertical splitting for Wall 3 did not propagate up the length of the lap until a comparatively late stage of testing (μ = 4.8). As a consequence, bond failure of tension steel at the wall ends was delayed, and damage to the comparatively short compression zones did not result in excessive strength degradation until μ = 4.8. Although this level of ductility (μ = 4.8) is much higher than predicted by the design charts, it should be noted that crushing and vertical splitting actually first occurred at μ = 1.6. Consequently, using the criterion of limiting ultimate strain, the available ductility would have been less than predicted.

Wall 2, which duplicated Wall 1 except for inclusion of confining plates in the end 600 mm of courses two to eight, exhibited greatly improved behaviour. Much less damage occurred to the compression zones, with the confining plates providing good restraint to the grout core, and minimising the tendency of the extreme tension bars to buckle in compression. As a consequence,bond failure of extreme tension reinforcement was inhibited.

Although maximum compression strains exceeded the suggested confined ultimate of 0.8% at a comparatively early stage of testing, Wall 2 did not fail the strength degradation criterion at μ = 7.9.

Figure 16 compares load vs cumulative ductility demand for the Walls 1 and 2. Cumulative ductility can be considered a more meaningful comparative than absolute ductility level because of the inevitable degradation occurring while cycling to a given level. Also plotted in Fig. 16 are the theoretical ultimate load of 272 kN, and the design ultimate load based on measured material strength and ϕ = 0.70 (appropriate for $N_u/f'_m Ag = 0.075$). It will be seen that for corresponding levels of strength degradation, Wall 2 was able to sustain approximately three times the cumulative ductility of Wall 1. Wall 2 exceeded the design ultimate capacity for all except one half cycle at μ = 5.68.

Influence of Lapping Vertical Reinforcement

Lapping of flexural starter bars in the plastic hinge region at the wall base had a profound influence on the behaviour of all three walls. Perhaps the most important effect was the reduction in equivalent plastic hinge length which resulted from the stiffening and strengthening influence of the doubled reinforcement ratio within the lap. This concentrated the plasticity into a very short region at the wall base, giving a plastic hinge length less than $0.2L_w$ at design levels of ductility. A consequence of this action was the high compression strain in the plastic hinge zone at comparatively low ductility, inducing premature vertical splitting of the compression zone.

A second undesirable effect of the lap was the tensile bond failures induced in tension reinforcement close to the wall end. This was initiated by the vertical splitting caused when the end of the wall had been in compression during a previous loading cycle. Splitting forces associated with transfer of tensile forces from starter to lapped bar propagated the vertical cracks and caused the bond failures.

In Wall 2, vertical splitting was inhibited by confining plates in critical mortar beds, and bond failure did not eventuate until the final stages of testing. In Wall 3, vertical splitting developed early in the test sequence, but did not propagate up the lap. This was presumably due to the increased lap length for Wall 3, though the reduced extent of the compression zone may have been a contributing factor. Until further data are available it is felt that the code lap length of $81d_b$ for Grade 380 reinforcement should be a minimum.

CONCLUSIONS

The wall tests showed that elastic properties and flexural strength of slender masonry shear walls can be predicted with good accuracy.

Results from the walls gave reasonable confirmation of theoretical ductility capacity charts developed in references 7 and 11 when allowance for the reduced plastic hinge length resulting from the lapping of flexural reinforcement was made. However, for Wall 3, degradation after masonry crushing first occurred was gradual. For lightly loaded walls use of ultimate crushing strain as an indicator of ductility capacity is felt to be conservative.

The walls clearly indicated that problems must be expected from lapping starter bars within plastic hinge regions. Whenever possible this should be avoided to increase the extent of plasticity, thus reducing peak compression strains for a given ductility, and eliminating bond problems. Testing, however, is urgently needed to better define ductility capacity of walls without lapping of vertical reinforcement in the plastic hinge zone.

Walls 1 and 2 violated slenderness requirements of the concrete and masonry design codes. Despite this there was no tendency of the compression zones to become laterally unstable. More testing is required to further test this aspect for walls where depth of compression at ultimate flexural strength is a greater proportion of wall length. The logical way to test this is in walls with lower masonry cursching strength f'_m. It has, however, been remarkably difficult to obtain low strength masonry, even when minimum strength materials are deliberately specified.

Finally, the walls confirm that ductility capacity is more of a problem for tall shear walls than for the squat walls previously tested, and capacity of many conventionally designed masonry shear walls

may be suspect. Use of confining plates within critical mortar courses at the ends of the wall in the potential plastic hinge zone will substantially improve response to severe seismic attack.

ACKNOWLEDGEMENTS

Grateful acknowledgement is made of financial assistance from the Ministry of Works and Development, the New Zealand Concrete Masonry Association and the University of Canterbury.

REFERENCES

1. Priestley, M.J.N. and Bridgeman, D.O., 'Seismic Resistance of Brick Masonry Walls', Bull. NZNSEE, Vol.7, No. 4, Dec. 1974, pp. 167-187.

2. Priestley, M.J.N., 'Seismic Resistance of Reinforced Concrete Masonry Shear Walls with High Steel Percentages', Bull. NZNSEE, Vol.10, No. 1, March 1977, pp.1-16.

3. Trounce, M.J. and Priestley, M.J.N., 'Seismic Behaviour of Reinforced Concrete Masonry Shear Walls', Department of Civil Engineering, University of Canterbury, Research Report 78-19, Feb. 1978, 112p.

4. Williams, D., 'Seismic Behaviour of Reinforced Masonry Shear Walls', Ph.D. Thesis, Department of Civil Engineering,University of Canterbury, 1971, 107p.

5. Mayes, R.L., Omote, Y. and Clough R.W., 'Cyclic Shear Tests of Masonry Piers Volume 1 - Test Result'. University of California, Berkeley, Earthquake Engineering Research Centre Report EERC 76-8, May 1976, 84p.

6. Hidalgo, P.A., Mayes, R.L., McNiven, H.D., and Clough, R.W., 'Cyclic Loading Tests of Masonry Single Piers' (3 vols.), University of California, Berkeley, Reports EERC 78-27, 78-28 and 29-12.

7. Priestley, M.J.N., 'Ductility of Unconfined Masonry Shear Walls', Bull. NZNSEE Vol. 14, No. 1, March 1981, pp.12-20.

8. - 'The Design of Concrete Structures', DZ3101, Standards Association of New Zealand, 1980.

9. - "The Design of Reinforced Masonry', DZ4210, Part B, SANZ, Wellington, 1980.

10. Priestley, M.J.N. and Elder, D.McG., 'Seismic Behaviour of Slender Masonry Shear Walls', Dept. of Civil Eng., University of Canterbury, Research Dept. (to be published).

11. Priestley, M.J.N.,'Ductility of Confined Masonry Shear Walls' Bull. NZNSEE, Vol.15, No.1, March 1982.

12. Hilsdorf, H.K., 'An Investigation into the Failure Mechanism of Brick Masonry Under Axial Compression', Designing, Engineering and Construction with Masonry Products, F.B. Johnston Ed., Gulf Pub. Co., Houston, Texas, Mag. 1969, pp. 34-41.